

Acoustic Signatures in the Primary Microwave Background Bispectrum

Eiichiro Komatsu* and David N. Spergel†

Department of Astrophysical Sciences, Princeton University, Princeton, NJ 08544, USA.

(Submitted to PRL – April 2000)

If the primordial fluctuations were non-Gaussian, then this non-Gaussianity should be apparent in the cosmic microwave background (CMB) sky. With their sensitive all-sky observation, MAP and Planck satellites should be able to detect weak non-Gaussianity in the CMB sky. On large angular scale, there is a linear relationship between the CMB temperature and the primordial curvature perturbation: $\Delta T/T = -\Phi/3$. On smaller scales; however, the radiation transfer function becomes more complex. In this Letter, we present the first results of computing the angular bispectrum of the primary CMB anisotropy that uses the full transfer function. We find that the bispectrum has a series of acoustic peaks with a period of acoustic oscillations twice as long as that of the angular power-spectrum. Using a single non-linear coupling parameter to characterize the amplitude of the bispectrum, we estimate the expected signal-to-noise ratio for COBE, MAP, and Planck experiments. To detect the non-Gaussianity by each experiment, we find that the coupling parameter should be larger than 500, 20, and 5, for COBE, MAP, and Planck, respectively. Since the simple inflationary scenarios predict that the parameter is an order of 0.01, the detection of non-Gaussianity by COBE, or future satellite experiments, would be problematic for those scenarios. The primary CMB bispectrum is a test of the inflationary scenario, and also a probe of the non-linear physics in the very early universe.

Why measure the bispectrum of the cosmic microwave background (CMB) radiation anisotropy? Simple inflationary models predict that the CMB anisotropy field is nearly random Gaussian, and that two-point statistics completely specify statistical properties of CMB. However, our universe may not be so simple. Higher order statistics, such as the three-point correlation function, or its harmonic transform, the angular bispectrum, are potential probes of the physics of generating the primordial fluctuations. Since gravitationally induced non-linearities are small at $z \sim 1300$, CMB is expected to be the best probe of the primordial non-Gaussianity [1].

In the inflationary scenario [2–5], the quantum fluctuations of the scalar (inflaton) field generate the observed matter and radiation fluctuations in the universe [6–9]. In the stochastic inflationary scenario of Starobinsky [10], the quantum fluctuations decohere to generate the classical fluctuations. There are two potential sources of non-Gaussianity in this inflationary model: (a) the non-linear coupling between the classical inflaton field and the observed fluctuation field, and (b) the non-linear coupling between the quantum noise field and the classical fluctuation field. The former has been investigated by Salopek and Bond [11], while the latter has been explored by Gangui et al. [12]. Calzetta and Hu [13] and Matacz [14] present an alternative treatment of the de-

coherence process that leads to different results for the primordial density perturbation from those obtained by Starobinsky [10]. Matacz’s treatment makes similar predictions for the level of non-Gaussianity to the Starobinsky’s treatment [15]. These studies conclude that in the slow roll regime, the fluctuations are Gaussian. However, features in the inflaton potential can produce significant non-Gaussianity [16].

There have been claims for both the non-detection [17] and the detection [18] of the non-Gaussianity in the COBE map. If the primordial fluctuations are Gaussian, then the gravitational lensing and the Sunyaev-Zel’dovich effect will produce weak, but potentially detectable, non-Gaussianity in the bispectrum [19–21]; however, the form of these terms should be easily distinguished from the primordial one. MAP and Planck will measure the fluctuation field down to angular scales $\simeq 0.2^\circ$ and 0.1° , and test these claims.

Previous work on the primordial non-Gaussianity has focused on very large angular scale, where the temperature fluctuations trace the primordial fluctuations. This is valid on the COBE scale. For MAP and Planck; however, we need the full effect of the radiation transfer function. In this Letter, we develop a formalism for doing this, and then present numerical results. Both the formalism and the numerical results are main results of this Letter.

The observed CMB temperature field $T(\hat{\mathbf{n}})$ can be expanded into the spherical harmonics: $a_{lm} \equiv \int d\hat{\mathbf{n}} T(\hat{\mathbf{n}}) Y_{lm}^*(\hat{\mathbf{n}})$, where hats denote unit vectors. The CMB angular bispectrum is given by $B_{l_1 l_2 l_3}^{m_1 m_2 m_3} \equiv \langle a_{l_1 m_1} a_{l_2 m_2} a_{l_3 m_3} \rangle$, and the angle-averaged bispectrum is

* komatsu@astro.princeton.edu; also at the Astronomical Institute, Tohoku University, Aoba, Sendai 980-8578, Japan.

†dns@astro.princeton.edu

defined by

$$B_{l_1 l_2 l_3} \equiv \sum_{m_1 m_2 m_3} \begin{pmatrix} l_1 & l_2 & l_3 \\ m_1 & m_2 & m_3 \end{pmatrix} B_{l_1 l_2 l_3}^{m_1 m_2 m_3}, \quad (1)$$

where the matrix is the Wigner-3j symbol. If the primordial fluctuations are adiabatic scalar fluctuations, then

$$a_{lm}(\mathbf{k}) = 4\pi(-i)^l \Phi(\mathbf{k}) g_{Tl}(k) Y_{lm}^*(\hat{\mathbf{k}}), \quad (2)$$

where $\Phi(\mathbf{k})$ is the primordial curvature perturbation, and $g_{Tl}(k)$ is the radiation transfer function. $a_{lm}(\mathbf{k})$ thus takes over the non-Gaussianity, if any, from $\Phi(\mathbf{k})$. Although equation (2) is valid only if the universe is flat, it is straightforward to extend this to arbitrary geometry. The isocurvature fluctuations can be similarly calculated by using the entropy perturbation and the proper transfer function.

In this letter, we explore the simplest case. We decompose $\Phi(\mathbf{k})$ into two parts: $\Phi(\mathbf{k}) = \Phi_L(\mathbf{k}) + \Phi_{NL}(\mathbf{k})$, where $\Phi_L(\mathbf{k})$ denotes the linear part of the perturbation, while $\Phi_{NL}(\mathbf{k})$ does the non-linear part defined by $\Phi_{NL}(\mathbf{k}) \equiv (2\pi)^{-3} f_{NL} \int d^3\mathbf{p} \Phi_L(\mathbf{k} + \mathbf{p}) \Phi_L^*(\mathbf{p})$. Henceforth, we shall call f_{NL} the non-linear coupling constant. In this model, the non-vanishing components of the $\Phi(\mathbf{k})$ -field bispectrum are,

$$\begin{aligned} & \langle \Phi_L(\mathbf{k}_1) \Phi_L(\mathbf{k}_2) \Phi_{NL}(\mathbf{k}_3) \rangle \\ &= 2(2\pi)^3 \delta^{(3)}(\mathbf{k}_1 + \mathbf{k}_2 + \mathbf{k}_3) f_{NL} P_\Phi(k_1) P_\Phi(k_2), \end{aligned} \quad (3)$$

where $P_\Phi(k)$ is the linear power-spectrum given by $\langle \Phi_L(\mathbf{k}_1) \Phi_L(\mathbf{k}_2) \rangle = (2\pi)^3 P_\Phi(k_1) \delta^{(3)}(\mathbf{k}_1 + \mathbf{k}_2)$. This model is based upon the slow-roll inflationary scenario. Salopek and Bond [11] and Gangui et al. [12] found that f_{NL} is given by a certain combination of the slope and the curvature of the inflaton potential. In the notation of Gangui et al., $\Phi_3 = 2f_{NL}$. Gangui et al. found that $\Phi_3 \sim 10^{-2}$ in the quadratic and the quartic inflaton potential models. If the slow-roll condition is not satisfied, then $f_{NL} = f_{NL}(k_1, k_2, k_3)$ at equation (3) [12]. Note that even if the inflation produced Gaussian fluctuations, Pyne and Carroll pointed out that the general relativistic second-order perturbation theory would produce terms of $f_{NL} \sim \mathcal{O}(1)$ [22]. For generic slow-roll models, these terms dominate the primordial non-Gaussianity.

Combining equation (2) and (3), we can obtain a compact expression for a component of the CMB angular bispectrum $B_{l_1 l_2 l_3}^{m_1 m_2 m_3}$,

$$\begin{aligned} & \langle a_{l_1 m_1}^L a_{l_2 m_2}^L a_{l_3 m_3}^{NL} \rangle \\ &= 2\mathcal{H}_{l_1 l_2 l_3}^{m_1 m_2 m_3} \int r^2 dr b_{l_1}^L(r) b_{l_2}^L(r) b_{l_3}^{NL}(r), \end{aligned} \quad (4)$$

where $\mathcal{H}_{l_1 l_2 l_3}^{m_1 m_2 m_3} \equiv \int d\hat{\mathbf{n}} Y_{l_1 m_1}^*(\hat{\mathbf{n}}) Y_{l_2 m_2}^*(\hat{\mathbf{n}}) Y_{l_3 m_3}^*(\hat{\mathbf{n}})$ is the geometrical factor, and

$$b_l^L(r) \equiv \frac{2}{\pi} \int k^2 dk P_\Phi(k) g_{Tl}(k) j_l(kr), \quad (5)$$

$$b_l^{NL}(r) \equiv \frac{2}{\pi} \int k^2 dk f_{NL} g_{Tl}(k) j_l(kr). \quad (6)$$

Note that $b_l^L(r)$ is a dimensionless quantity, while $b_l^{NL}(r)$ has a dimension of L^{-3} . We compute the radiation transfer function $g_{Tl}(k)$ with the CMBFAST [23] code, and assume the single power-law spectrum, $P_\Phi(k) \propto k^{n-4}$, for the primordial curvature fluctuations. We can see that the bispectrum is fully specified by a single parameter f_{NL} , as the cosmological parameters will be precisely determined by measuring the CMB angular power-spectrum C_l (e.g., [24]). It should be stressed again that this is the special case in the slow-roll limit. More generic case will be treated in future publications.

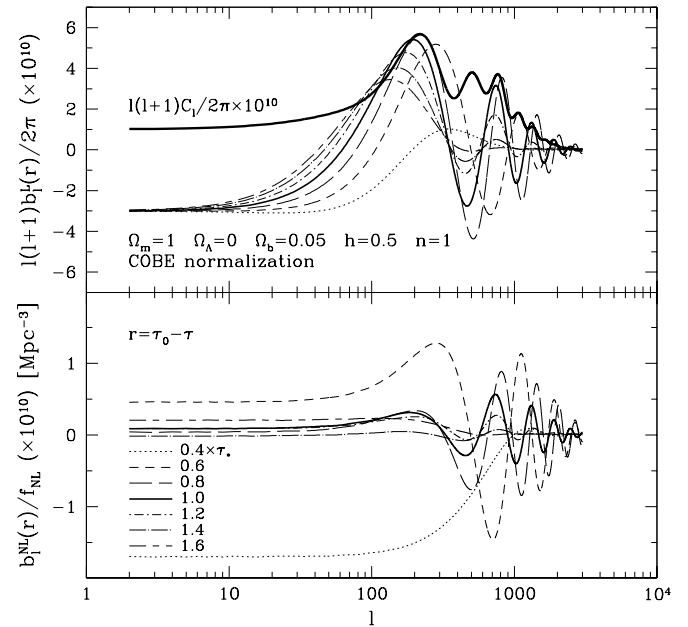


FIG. 1. This figure shows $b_l^L(r)$ and $b_l^{NL}(r)$, the two terms in our calculation of the CMB angular bispectrum, as a function of r (see Eq.(5) and (6) for definition). Various lines in the upper panel show $[l(l+1)b_l^L(r)/2\pi] \times 10^{10}$, where $r = \tau_0 - \tau$, at $\tau = 0.4, 0.6, 0.8, 1.0, 1.2, 1.4$, and $1.6 \times \tau_*$ (decoupling time), while $[b_l^{NL}(r)/f_{NL}] \times 10^{10}$ are shown in the lower panel. τ_0 is the present-day conformal time. Note that $\tau_0 = 11.8$ Gpc, and $\tau_* = 235$ Mpc in our cosmological model chosen here. The thickest solid line in the upper panel is the CMB angular power-spectrum $[l(l+1)C_l/2\pi] \times 10^{10}$. C_l is shown for comparison.

Figure 1 shows $b_l^L(r)$ and $b_l^{NL}(r)$ for several different values of r . The cosmological model chosen here is the scale-invariant standard cold dark matter model with $\Omega_m = 1$, $\Omega_\Lambda = 0$, $h = 0.5$, and $n = 1$, and with the power-spectrum $P_\Phi(k)$ normalized to COBE [25]. Although this model is almost excluded by current observations, it is still useful to depict the basic effects of the transfer function on the bispectrum. $r = \tau_0 - \tau$, where τ is the conformal time, and τ_0 is the one at the present. In our model, $\tau_0 = 11.8$ Gpc, and the decoupling epoch occurs

at $\tau_* = 235$ Mpc at which the differential visibility has a maximum. $b_l^L(r)$ and C_l look very similar each other, the shape and the amplitude in $l \gtrsim 100$, although the amplitude in the Sachs–Wolfe regime is different by a factor of -3 . This is because C_l is proportional to $P_\Phi(k)g_{Tl}^2(k)$, while $b_l^L(r) \propto P_\Phi(k)g_{Tl}(k)$, where $g_{Tl} = -1/3$. In addition, the main difference between C_l and $b_l(r)$ is that $b_l(r)$ can change the sign, while C_l cannot. $b_l^L(r)$ has a good phase coherence over wide range of r , while the phase of $b_l^{NL}(r)$ in high- l regime oscillates rapidly as a function of r . This strongly damps the integrated result of the bispectrum (Eq.4) in high- l regime.

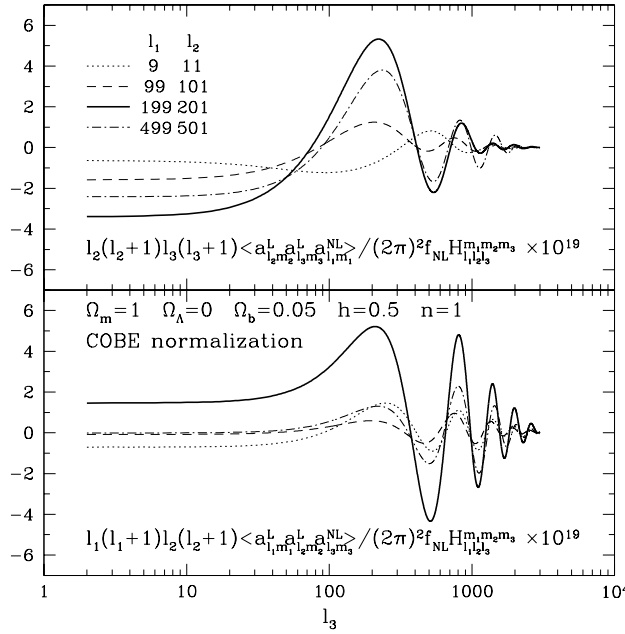


FIG. 2. The CMB angular bispectrum, with the geometrical factor $\mathcal{H}_{l_1 l_2 l_3}^{m_1 m_2 m_3}$ excluded. The upper panel shows $[l_2(l_2+1)l_3(l_3+1)\langle a_{l_2 m_2}^L a_{l_3 m_3}^L a_{l_1 m_1}^{NL} \rangle / (2\pi)^2 f_{NL} \mathcal{H}_{l_1 l_2 l_3}^{m_1 m_2 m_3}] \times 10^{19}$, while the lower panel shows $[l_1(l_1+1)l_2(l_2+1)\langle a_{l_1 m_1}^L a_{l_2 m_2}^L a_{l_3 m_3}^{NL} \rangle / (2\pi)^2 f_{NL} \mathcal{H}_{l_1 l_2 l_3}^{m_1 m_2 m_3}] \times 10^{19}$. Those are shown as functions of l_3 for $(l_1, l_2) = (9, 11), (99, 101), (199, 201)$, and $(499, 501)$.

Figure 2 shows the integrated bispectrum (Eq.(4)), with the geometrical factor $\mathcal{H}_{l_1 l_2 l_3}^{m_1 m_2 m_3}$ excluded. Since the signal comes primarily from the decoupling epoch, the integration boundary is chosen as $\tau_0 - 2\tau_* \leq r \leq \tau_0 - 0.1\tau_*$. We use a step-size of $0.1\tau_*$, as we found that a step size of $0.01\tau_*$ gives very similar results. While the bispectrum is a 3-d function, we show different 1-d slices of the bispectrum in this figure. $\langle a_{l_2 m_2}^L a_{l_3 m_3}^L a_{l_1 m_1}^{NL} \rangle$ is plotted as a function of l_3 in the upper panel, while $\langle a_{l_1 m_1}^L a_{l_2 m_2}^L a_{l_3 m_3}^{NL} \rangle$ is plotted in the lower panel. l_1 and l_2 are chosen so as $(l_1, l_2) = (9, 11), (99, 101), (199, 201)$, and $(499, 501)$. We find that the $(l_1, l_2) = (199, 201)$ mode, the first acoustic peak mode, has the largest sig-

nal in this family of parameters. The upper panel has a prominent first acoustic peak, and strongly damped oscillations in high- l regime. The lower panel also has a first peak, but damps more slowly. The typical amplitude of the bispectrum is $l^4 \langle a_{l m}^3 \rangle / f_{NL} \sim 10^{-18}$. Since $l^2 b_l^L$ has a comparable amplitude to $l^2 C_l$ (see figure 1), $l^2 b_l^L \sim 10^{-9}$. Looking at the lower panel of figure 1, we also find $b_l^{NL} / f_{NL} \sim 10^{-10} \text{ Mpc}^{-3}$. The most signal coming from the decoupling, the volume element at τ_* is $r_*^2 \Delta r_* \sim (10^4)^2 \times 10^2 \text{ Mpc}^3$, and thus $l^4 \langle a_{l m}^3 \rangle / f_{NL} \sim r_*^2 \Delta r_* (l^2 b_l^L)^2 b_l^{NL} / f_{NL} \sim 10^{-18}$. Since $b_l^{NL} / f_{NL} \sim r_*^{-2} \delta(r - r_*)$, $r_*^2 \Delta r_* b_l^{NL} / f_{NL} \sim 1$. Our numerical results of the bispectrum agree with Gangui et al. [12] calculation in the Sachs–Wolfe regime, where $\langle a_{l_2 m_2}^L a_{l_3 m_3}^L a_{l_1 m_1}^{NL} \rangle \simeq -6 f_{NL} C_{l_2} C_{l_3} \mathcal{H}_{l_1 l_2 l_3}^{m_1 m_2 m_3}$ in the upper panel of figure 2, and $\langle a_{l_1 m_1}^L a_{l_2 m_2}^L a_{l_3 m_3}^{NL} \rangle \simeq -6 f_{NL} C_{l_1} C_{l_2} \mathcal{H}_{l_1 l_2 l_3}^{m_1 m_2 m_3}$ in the lower panel. This comparison is only valid when l_1, l_2 , and l_3 are all less than ~ 10 , where Gangui et al.’s formula gives $\simeq -6 \times 10^{-20}$.

Finally, we shall discuss the detectability of CMB experiments to the primordial non-Gaussianity in the bispectrum. We estimate the signal-to-noise ratio (S/N) of a detection by computing,

$$\chi^2 \equiv \sum_{2 \leq l_1 \leq l_2 \leq l_3} \frac{B_{l_1 l_2 l_3}^2}{\sigma_{l_1 l_2 l_3}^2}. \quad (7)$$

χ^2 roughly corresponds to $(S/N)^2$ (see [19]). The variance $\sigma_{l_1 l_2 l_3}^2 \equiv \langle B_{l_1 l_2 l_3}^2 \rangle$ is given by $C_{l_1} C_{l_2} C_{l_3} \Delta_{l_1 l_2 l_3}$ [19,26], where $\Delta_{l_1 l_2 l_3}$ takes values 1, 2, and 6 for cases of that all l ’s are different, two of them are same, and all are same, respectively. $C_l \equiv C_l + C_l^N$ is the total CMB angular power-spectrum, which includes the power-spectrum of the detector noise C_l^N . C_l^N is calculated analytically using the formula derived by Knox [27] with the noise characteristics of the relevant experiments. The angle-averaged bispectrum $B_{l_1 l_2 l_3}$ can be computed using the following identity:

$$\sum_{m_1 m_2 m_3} \begin{pmatrix} l_1 & l_2 & l_3 \\ m_1 & m_2 & m_3 \end{pmatrix} \mathcal{H}_{l_1 l_2 l_3}^{m_1 m_2 m_3} = \sqrt{\frac{(2l_1+1)(2l_2+1)(2l_3+1)}{4\pi}} \begin{pmatrix} l_1 & l_2 & l_3 \\ 0 & 0 & 0 \end{pmatrix}. \quad (8)$$

This function is non-zero only if the triangle conditions: $l_1 + l_2 + l_3 = \text{even}$, and $|l_i - l_j| \leq l_k \leq l_i + l_j$ for all permutations of indices, are all satisfied.

Figure 3 shows the differential χ^2 at $\ln l_3$ interval, $d\chi^2 / d \ln l_3$, in the upper panel, and $\chi^2(< l_3)$, which is χ^2 summed up to a certain l_3 , in the lower panel. The detector noises C_l^N have been computed for COBE 4-yr results [28], for MAP 90 GHz channel, and for Planck 217 GHz channel, but the effect of limited sky coverage is neglected. Figure 3 also shows $d\chi^2 / d \ln l_3$ and $\chi^2(< l_3)$ for the “ideal” experiment with no noise: $C_l^N = 0$. Both $d\chi^2 / d \ln l_3$ and $\chi^2(< l_3)$ are monotonically increasing function with l_3 , roughly $\propto l_3^2$ up to $l_3 \sim 2000$, for the

ideal experiment. Since the number of modes increases as l^3 and $l \begin{pmatrix} l & l & l \\ 0 & 0 & 0 \end{pmatrix}^2$ nearly scales as l^{-1} , $\chi^2/f_{NL}^2 \sim l^3 \times l \begin{pmatrix} l & l & l \\ 0 & 0 & 0 \end{pmatrix}^2 \times (l^4 \langle a_{lm}^3 \rangle / f_{NL} \mathcal{H}_{lll}^{mmm})^2 / (l^2 C_l)^3 \sim l^2 \times 10^{-9}$. Beyond $l_3 \sim 2000$, an enhancement of the damping tail in C_l because of the weak lensing effect [29] stops $d\chi^2/d\ln l_3$ increasing. For a given experiment, $d\chi^2/d\ln l_3$ has a maximum at a scale near the beam-size.

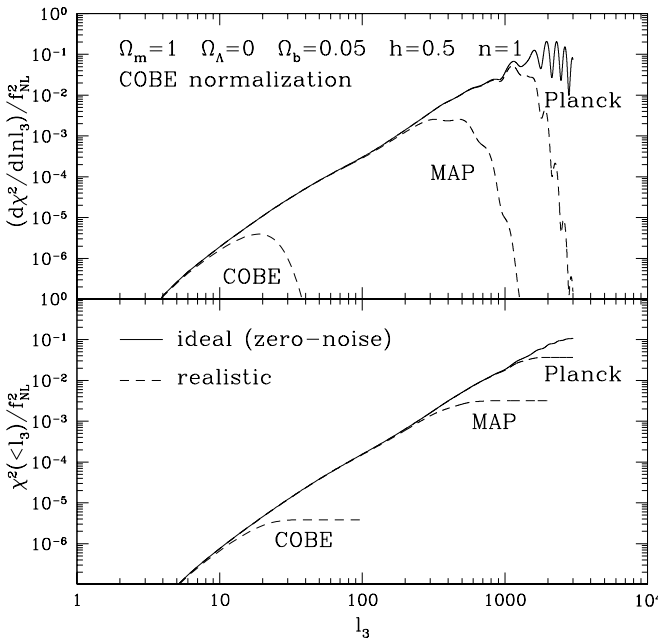


FIG. 3. The predictions of the square of effective signal-to-noise ratio, $\chi^2 \simeq (S/N)^2$, for COBE, MAP, and Planck experiments (see Eq.(7)). The differential statistic in the upper panel, while the cumulative statistic up to a certain l_3 is shown in the lower panel. Both are in units of f_{NL}^2 . Solid line represents the zero-noise “ideal” experiment, while dotted lines show the realistic experiments mentioned above. The total χ^2/f_{NL}^2 are 3.9×10^{-6} , 3.2×10^{-3} , and 3.8×10^{-2} for COBE, MAP, and Planck experiments, respectively.

The total χ^2/f_{NL}^2 are 3.9×10^{-6} for the COBE results, and 3.2×10^{-3} and 3.8×10^{-2} , for MAP and Planck, respectively. To obtain $S/N > 1$, therefore, we need $f_{NL} > 500, 20$, and 5 for each corresponding experiment.

The simplest inflationary scenario usually predicts small f_{NL} ($\sim 10^{-2}$) which is below the detection limit even of an “ideal” noise-free experiment. On the other hand, if the reported detection [18] of the non-Gaussianity in the COBE map were correct, then MAP and Planck would detect strong signals of the non-Gaussianity.

We would thank Naoshi Sugiyama for useful comments. E. K. acknowledges a fellowship from the Japan

Society for the Promotion of Science. D. N. S. is partially supported by the MAP/MIDEX program.

[1] L. Verde, L. Wang, A. F. Heavens and M. Kamionkowski, Mon. Not. R. Astron. Soc. **313**, 141 (2000).
[2] K. Sato, Mon. Not. R. Astron. Soc. **195**, 467 (1981); Phys. Lett. **99B**, 66 (1981).
[3] A. Guth, Phys. Rev. D **23**, 347 (1981).
[4] A. Albrecht and P. J. Steinhardt, Phys. Rev. Lett. **48**, 1220 (1982).
[5] A. D. Linde, Phys. Lett. **108B**, 389 (1982).
[6] A. Guth and S. Y. Pi, Phys. Rev. Lett. **49**, 1110 (1982).
[7] S. Hawking, Phys. Lett. **115B**, 295 (1982).
[8] J. M. Bardeen, P. J. Steinhardt and M. S. Turner, Phys. Rev. D **28**, 679 (1983).
[9] A. A. Starobinsky, Phys. Lett. **117B**, 175 (1982).
[10] A. A. Starobinsky, in *Field Theory, Quantum Gravity, and Strings*, edited by H. T. de Vega and N. Sanchez, Lecture Notes in Physics, Vol. 246 (Springer-Verlag, Berlin, 1986), p.107.
[11] D. S. Salopek and J. R. Bond, Phys. Rev. D **42**, 3936 (1990); *ibid.* **43**, 1005 (1991).
[12] A. Gangui, F. Lucchin, S. Matarrese and S. Mollerach, Astrophys. J. **430**, 447 (1994).
[13] E. Calzetta and B. L. Hu, Phys. Rev. D **52**, 6770 (1995).
[14] A. Matacz, Phys. Rev. D **55**, 1860 (1997).
[15] A. Matacz, Phys. Rev. D **56**, R1836 (1997).
[16] L. Kofman, G. R. Blumenthal, H. Hodges and J. R. Primack, in *Large-Scale Structures and Peculiar Motions in the Universe*, edited by D. W. Latham and L. N. daCosta, ASP Conference Series, Vol. 15, 1991, p.339.
[17] A. Kogut, A. J. Banday, C. L. Bennett, K. M. Gorski, G. Hinshaw, G. F. Smoot and E. L. Wright, Astrophys. J. Lett. **464**, L29 (1996).
[18] P. G. Ferreira, J. Magueijo and K. M. Gorski, Astrophys. J. Lett. **503**, L1 (1998).
[19] D. N. Spergel and D. M. Goldberg, Phys. Rev. D **59**, 103001 (1999).
[20] D. M. Goldberg and D. N. Spergel, Phys. Rev. D **59**, 103002 (1999).
[21] A. Cooray and W. Hu, preprint, astro-ph/9910397.
[22] T. Pyne and S. M. Carroll, Phys. Rev. D **53**, 2920 (1996).
[23] U. Seljak and M. Zaldarriaga, Astrophys. J. **469**, 437 (1996).
[24] J. R. Bond, G. Efstathiou and M. Tegmark, Mon. Not. R. Astron. Soc. **291**, L33 (1997).
[25] E. F. Bunn and M. White, Astrophys. J. **480**, 6 (1997).
[26] X. Luo, Astrophys. J. Lett. **427**, L71 (1994).
[27] L. Knox, Phys. Rev. D **48**, 3502 (1995).
[28] C. L. Bennett, et al., Astrophys. J. Lett. **464**, L1 (1996).
[29] U. Seljak, Astrophys. J. **463**, 1 (1996).